

Super-luminous Supernova Remnants

By YOU-HUA CHU, C.-H. ROSIE CHEN
AND SHIH-PING LAI

Astronomy Department, University of Illinois, 1002 W. Green St., Urbana, IL 61801, USA

Some extragalactic SNRs are more than two orders of magnitude more luminous than the young Galactic SNR Cas A. These SNRs are called super-luminous or ultra-luminous SNRs. Their high luminosities can be caused by chance superpositions of multiple objects, interactions with a very dense environment, or unusually powerful supernova explosions. Four super-luminous SNRs are known: one in NGC 4449, one in NGC 6946, and two in M101. The two remnants in M101, NGC 5471B and MF83, are recently suggested to be “hypernova remnants” possibly connected to the GRBs. We have obtained new or archival HST WFPC2 images and new high-dispersion echelle spectra of these super-luminous SNRs, in order to examine their stellar and interstellar environments and to analyze their energetics. We discuss the physical nature of these four SNRs, with a special emphasis on the two “hypernova remnants” in M101.

1. Introduction

Supernova remnants (SNRs) usually exhibit three distinguishing characteristics: non-thermal radio emission, bright X-ray emission, and large optical [S II]/H α line ratios. These characteristics have been used as identification criteria for SNRs. In the Galaxy, SNRs are most effectively surveyed at radio wavelengths because heavy extinction in the Galactic plane hampers optical and X-ray observations (e.g., Green 1988). In the Magellanic Clouds, where interstellar extinction is small, SNRs can be surveyed at radio, X-ray, or optical wavelengths (Mathewson et al. 1983, 1984, 1985; Smith 1999). In distant galaxies, the sensitivity of available radio and X-ray instruments becomes a limiting factor; thus, surveys of SNRs are carried out in the optical (e.g., D’Odorico, Dopita, & Benvenuti 1980; Blair & Long 1997; Matonick & Fesen 1997).

Only a small number of the optically identified extragalactic SNR candidates can be confirmed at radio or X-ray wavelengths. These confirmed SNRs are among the most luminous remnants. In fact, some of them are so luminous that they were first identified in radio or X-rays and subsequently confirmed by optical spectroscopic observations. These luminous SNRs are often more than two orders of magnitude more luminous than the young Galactic SNR Cas A, and hence they have been called super-luminous or ultra-luminous SNRs.

Several factors may contribute to the brightness of extragalactic super-luminous SNRs. First, they might be composite objects, with X-ray binaries contributing to the X-ray emission, multiple SNRs contributing to the radio emission, or H II regions contributing to the H α emission. Second, these SNRs might be interacting with a very dense circumstellar or interstellar environment. As optical and X-ray emissions are dependent on (density)² \times (volume) and the energy is dependent on (density) \times (volume), for the same amount of energy, a greater amount of emission can be generated if the density is high. Finally, unusually powerful supernova explosions produce more energetic SNRs which may generate more emission and become super-luminous SNRs. For example, two super-luminous SNRs in M101 have been suggested to be “hypernova remnants” that require explosion energies as large as 10^{53} – 10^{54} ergs (Wang 1999).

In this paper, we report our analysis of four super-luminous SNRs. Two of these four remnants are the “hypernova remnants” in M101, and they are the main emphasis of

SNRs	Distance (Mpc)	L(X) (10^{36} erg/s)	L(408 MHz) (Cas A)	L(H α) (10^{37} erg/s)	Size (pc)
Cas A	0.003	3	1	—	4
NGC 4449	5	800	25	< 0.15	< 0.6
NGC 6946	5.1	2800	1	19	20 \times 30
NGC 5471B	7.2	170	3	160	60
MF83	7.2	100	—	17	267

TABLE 1. Super-luminous Supernova Remnants

this paper. We have obtained high-resolution images to examine the nebular morphology and stellar content, and high-dispersion spectra to determine the expansion velocity and kinetic energy. These new observations allow us to investigate the emission mechanisms and whether unusually energetic supernova explosions are needed for these remnants.

2. Super-luminous Supernova Remnants

Four super-luminous SNRs have been reported: one in NGC 4449 (Kirshner and Blair 1980), one in NGC 6946 (Schlegel 1994; Blair & Fesen 1994; Van Dyk et al. 1994), and two in M101 (Matonick & Fesen 1998; Wang 1999). The X-ray, radio, and optical H α luminosities of these four remnants and Cas A (for comparison) are listed in Table 1. The numbers in Table 1 are taken from the above cited references and this paper. The radio luminosity at 408 MHz has been normalized to Cas A for easy comparisons.

It is clear from Table 1 that these super-luminous SNRs are most remarkable in the X-ray. The SNR in NGC 4449 is the smallest, the SNR in NGC 6946 has the highest X-ray luminosity, NGC 5471B has the highest H α luminosity, and MF83 is the largest.

3. Observations and Datasets

We intend to determine the physical nature of these super-luminous SNRs and the causes of their high luminosities. Useful optical observations for this study include high-resolution images and high-dispersion spectra. High-resolution images in the continuum bands can be used to study the stellar environment of a remnant, while flux-calibrated H α images can be used to determine the H α luminosity and rms electron density of the remnant. The [S II]/H α ratio map can be used to examine the spatial extent of the SNR shocks. High-dispersion spectra are useful in separating shocked and unshocked components, determining expansion and shock velocities, and measuring diagnostic nebular line ratios.

We have used the following datasets for the analysis presented in this paper:

- (1) HST FOC [O III] image of the SNR in NGC 4449 (archival);
- (2) HST WFPC2 H α , [S II], and continuum images of the SNR in NGC 6946 (archival), NGC 5471B (proprietary);
- (3) MDM 2.4m B, V, I, and H α images of MF83 (courtesy of Eva Grebel); and
- (4) KPNO 4m echelle spectra of the SNR in NGC 6946, NGC 5471B, and MF83 (proprietary).

We have adopted the analysis of the super-luminous SNR in NGC 4449 by Blair & Fesen (1998), but carried out our own analysis for the other three super-luminous SNRs. The detailed analysis and final results will be reported later in refereed journals.

4. The Super-luminous SNR in NGC 4449

The super-luminous SNR in NGC 4449 ($\alpha_{2000} = 12^{\text{h}}28^{\text{m}}10^{\text{s}}.9$, $\delta_{2000} = +44^{\circ}06'47''.7$) was first diagnosed by its nonthermal radio emission (Seaquist & Bignell 1978). Subsequent spectroscopic observations show narrow emission lines belonging to an HII region and broad emission lines of oxygen that are associated with dense supernova ejecta (Kirshner & Blair 1980). The widths of these oxygen emission lines suggest an expansion velocity of $3,500 \text{ km s}^{-1}$. The absence of broad $[\text{O II}]\lambda 3727$ emission indicates an electron density greater than 10^5 cm^{-3} , and the $[\text{O III}]\lambda 4363$ and $\lambda 5007$ line ratio implies an electron temperature of $\sim 40,000 \text{ K}$. These properties strongly point to a case of young SNR dominated by oxygen-rich ejecta of a supernova from a progenitor of mass $> 25 M_{\odot}$. The expansion of the high-density supernova ejecta into an HII region is responsible for the $\sim 10^{39} \text{ erg s}^{-1}$ X-ray luminosity (Blair, Kirshner, & Winkler 1983).

The super-luminous SNR in NGC 4449 has been recently studied by Blair & Fesen (1998) with high-resolution images taken with the HST Faint Object Camera (FOC), and with high-S/N spectra taken with the HST Faint Object Spectrograph and the 2.4m telescope at the MDM Observatory. The HST FOC images show that the SNR is unresolved by the point spread function of the HST (Figure 1), placing an upper limit of $0''.028$ (or 0.6 pc) on its diameter. The new spectra show broad wings of many emission lines indicating expansion velocities greater than $6,000 \text{ km s}^{-1}$. Blair and Fesen conclude that the super-luminous SNR in NGC 4449 is less than 100 years old, and that its high luminosity is owed to its youth and expansion into a dense circumstellar environment.

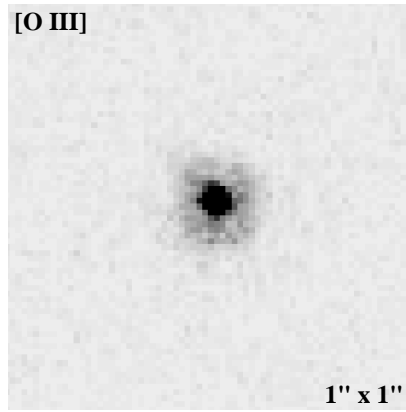


FIGURE 1. HST FOC $[\text{O III}]\lambda 5007$ image of the super-luminous SNR in NGC 4449. The image is unresolved and shows basically the point spread function of the HST. The field of view is $1'' \times 1''$ ($1'' = 24 \text{ pc}$).

5. The Super-luminous SNR in NGC 6946

The super-luminous SNR in NGC 6946 ($\alpha_{2000} = 20^{\text{h}}35^{\text{m}}00^{\text{s}}.75$, $\delta_{2000} = +60^{\circ}11'30''.6$) was initially identified in an optical survey (Blair & Fesen 1994). It was immediately obvious that this SNR is associated with an extremely luminous X-ray source. With an X-ray luminosity of $2.8 \times 10^{39} \text{ ergs s}^{-1}$, this SNR in NGC 6946 has the highest X-ray luminosity among all known SNRs (Schlegel 1994). Radio observations show that this SNR is three times as luminous as Cas A (Van Dyk et al. 1994). Such high luminosities are often associated with young SNRs; however, no high-velocity gas with expansion velocity greater than 600 km s^{-1} is detected (Blair & Fesen 1994).

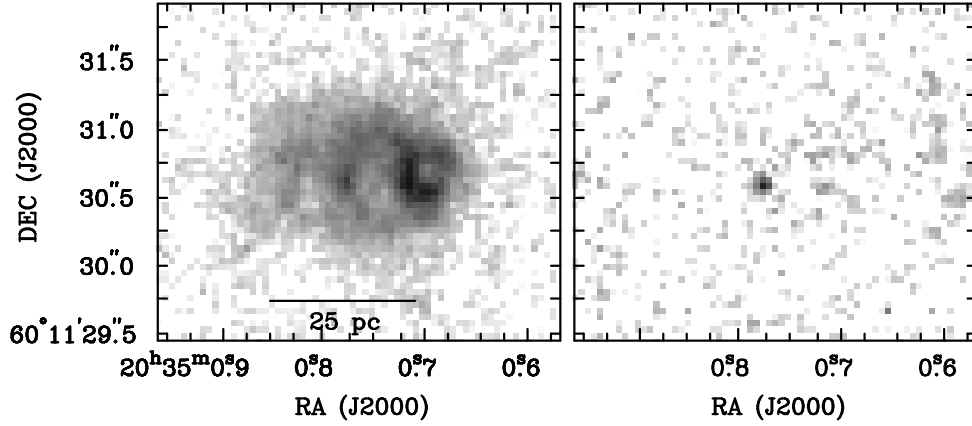


FIGURE 2. HST WFPC2 images of the super-luminous SNR in NGC 6946 in $H\alpha$ (left) and F439W blue continuum (right). These images are downloaded from the HST archive and plotted by Bryan Dunne.

HST Wide Field Planetary Camera 2 (WFPC2) images of the super-luminous SNR in NGC 6946 were recently reported by Blair, Fesen, & Schlegel (1997). The WFPC2 $H\alpha$ (F656N filter) image shows that this SNR is in an isolated environment and that the remnant has a multiple-loop morphology with an oblong outermost shell 20×30 pc in size (Figure 2). Based on this morphology, Blair et al. suggested that the high X-ray luminosity is caused by colliding SNRs, with the small, bright loop (~ 8 pc in diameter) on the western part being a young SNR and the outermost shell being an older SNR.

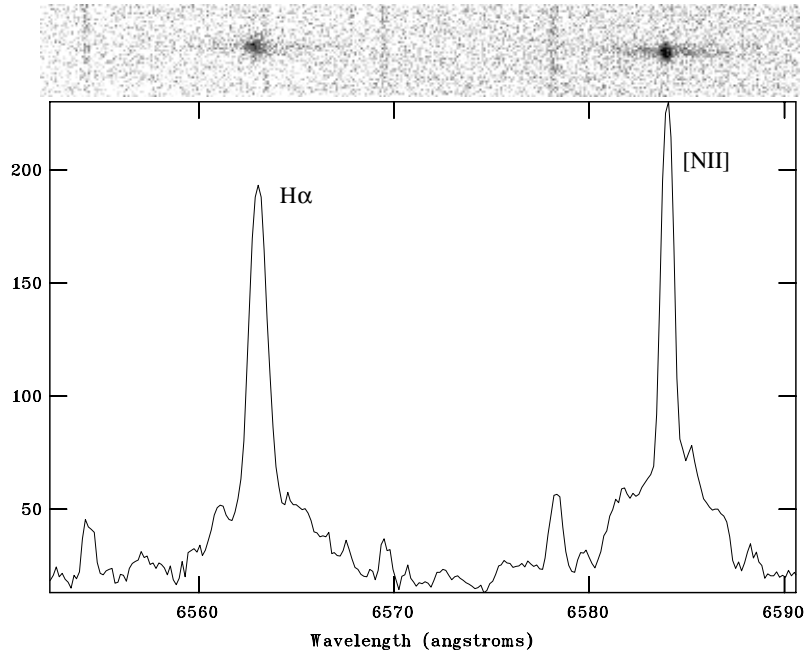


FIGURE 3. KPNO 4m echelle spectra of the super-luminous SNR in NGC 6946 in the region of $H\alpha$ and $[N II]$ lines. Both lines show a narrow component superposed on a broad component. The weak narrow lines are the geocoronal $H\alpha$ and telluric OH lines.

		Broad component	Narrow Component
H α	FWHM (km s ⁻¹)	285	42
[N II]	FWHM (km s ⁻¹)	250	25
H α	FWZI (km s ⁻¹)	450	...
[N II]	FWZI (km s ⁻¹)	400	...
[N II]/H α flux ratio		1.0	0.8
H α ,	broad/narrow flux ratio	1.5	...
[N II],	broad/narrow flux ratio	1.8	...

TABLE 2. H α and [N II] Lines of the Super-luminous SNR in NGC 6946

To investigate the kinematic properties of the super-luminous SNR in NGC 6946, we have obtained high-dispersion spectra using the echelle spectrograph on the 4m telescope at Kitt Peak National Observatory (Dunne, Gruendl, & Chu 1999). As shown in Figure 3, the nebular emission lines are resolved into a narrow component superposed on a broad component. The velocity width and [N II] λ 6583/H α line ratio can be measured separately for the broad component and the narrow component. These measurements are listed in Table 2.

The broad component must originate in SNR shocked material, while the narrow component consists of unshocked gas. The base of the broad component, the full width at zero intensity (FWZI), of the H α line extends over 450 km s⁻¹, indicating an expansion velocity of at least 225 km s⁻¹. This expansion velocity is not particularly high compared to those of SNRs in the Large Magellanic Cloud (Chu & Kennicutt 1988), and is usually associated with SNRs that are $\sim 10^4$ yrs old. The lack of material expanding at higher velocities is inconsistent with the identification of the bright, small (8-pc across) loop as a young SNR. The simple stellar environment, shown by the WFPC2 blue continuum image in Figure 2, also does not support a high supernova occurrence rate. It is thus not likely that the super-luminous SNR in NGC 6946 consists of colliding SNRs.

An effective clue to the nature of the super-luminous SNR in NGC 6946 is provided by the [N II]/H α ratios measured in the echelle spectrum. The [N II]/H α ratio is 0.8 in the narrow component and 1.0 in the broad component. An [N II]/H α ratio of 0.8 is hardly ever seen in an interstellar HII region, but is frequently seen in ring nebulae around Wolf-Rayet (WR) stars or luminous blue variables (LBVs). The [N II] line is strong because the nebulae contain N-rich material ejected by the central stars. It is possible that the progenitor of the supernova in NGC 6946's super-luminous SNR was a WR or LBV star, and the supernova ejecta interact with the dense circumstellar nebula and produce the high luminosity (Dunne et al. 1999).

The H α emission from the SNR shocked material can be determined from the flux contained in the broad component of the velocity profile. Assuming that the SNR shocked material is distributed in a shell whose thickness is 1% of its radius, Dunne et al. (1999) have derived a rms electron density of ~ 185 cm⁻³, a mass of $\sim 1,300$ M $_{\odot}$, and a kinetic energy of $\sim 7 \times 10^{50}$ ergs for the SNR shell. This kinetic energy is somewhat high, but does not need an explosion energy as high as those provided by GRBs.

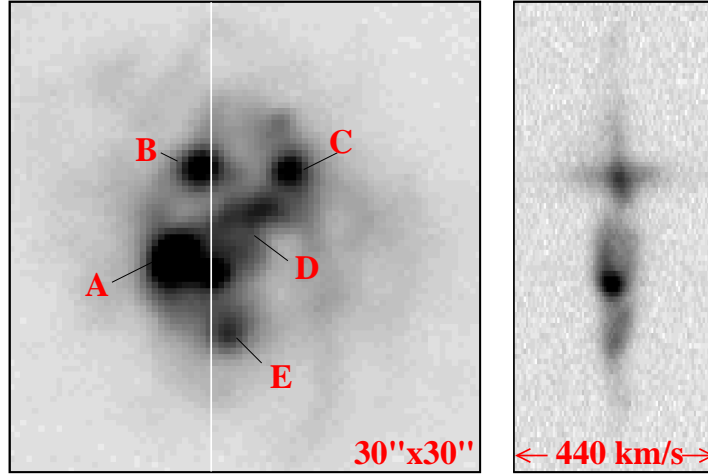


FIGURE 4. KPNO 2.1m $H\alpha$ CCD image of NGC 5471 (left) and KPNO 4m echelle $H\alpha$ line image (right), plotted with the same image scale. The A–E components of NGC 5471 and the echelle slit position are marked on the CCD image. The field of view of this image is $30'' \times 30''$ ($1'' = 35$ pc). The echelle $H\alpha$ line image covers 440 km s^{-1} along the X-axis. The broad emission component is clearly seen at the B component of NGC 5471.

6. The Super-luminous SNR NGC 5471B in M101

NGC 5471B is the B component of the giant HII region NGC 5471 in M101. The super-luminous SNR of NGC 5471B was initially discovered by its nonthermal radio emission and confirmed by its high $[S \text{ II}]/H\alpha$ ratio (Skillman 1985). High-dispersion echelle spectroscopic observations clearly show a broad emission line component at NGC 5471B (Figure 4). Using the high-dispersion echelle spectra, Chu & Kennicutt (1986) decomposed the $H\alpha$ velocity profile into a broad SNR component and a narrow HII region component, and derived a mass of $6,500 \pm 3,000 M_{\odot}$ and a kinetic energy of $(2.5 \pm 1) \times 10^{50}$ ergs for the SNR. ROSAT observations of NGC 5471 show an X-ray source centered at the B component with a luminosity of $3 \times 10^{38} \text{ ergs s}^{-1}$ (Williams & Chu 1995; Wang 1999). From this X-ray luminosity, Wang (1999) derived a supernova explosion energy of $\sim 3 \times 10^{52}$ ergs, and suggested that NGC 5471B is a “hypernova remnant”.

To study the physical nature of NGC 5471B, we have obtained HST WFPC2 images in $H\alpha$ (F656N), $[S \text{ II}]$ (F673N), and continuum bands (F547M and F675W). Comparisons between the $H\alpha$ and $[S \text{ II}]$ images of NGC 5471 show three shells with enhanced $[S \text{ II}]/H\alpha$ ratios (Figure 5). The brightest of these $[S \text{ II}]$ -bright shells is the super-luminous SNR in the B component.

A closer examination of NGC 5471B (Figure 6) shows that the super-luminous SNR is embedded in a very complex environment. The $H\alpha$ image shows roughly a shell structure, with a bright compact HII region at the southeast rim. The blue continuum (F547M) image shows individual supergiants, OB associations, and clusters. The compact HII region on the shell rim is coincident with an OB association/cluster. The $[S \text{ II}]$ image shows the brightest $[S \text{ II}]$ emission on the western side of the shell, where the underlying stellar emission is the lowest. The areas of enhanced $[S \text{ II}]/H\alpha$ ratio extend beyond the southwest rim of the shell.

To study the physical properties of the super-luminous SNR in NGC 5471B, it is necessary to separate the SNR emission from the background HII region emission. This can be achieved kinematically, using high-dispersion spectra. We have obtained new observations of NGC 5471 with the echelle spectrograph on the KPNO 4m telescope in

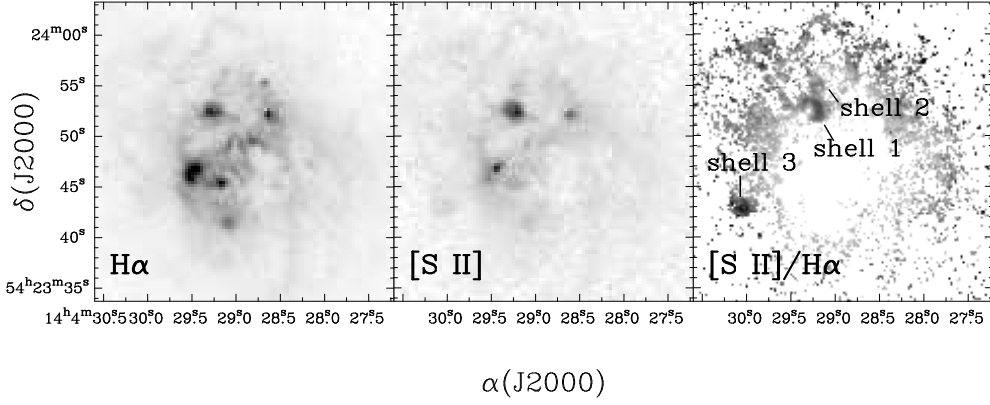


FIGURE 5. HST WFPC2 images of NGC 5471. The left two images are in $H\alpha$ and $[S II]$ lines, respectively. The right panel shows the $[S II]/H\alpha$ ratio map. The three $[S II]$ -enhanced shells are labeled. Shell 1 is the super-luminous SNR in NGC 5471B.

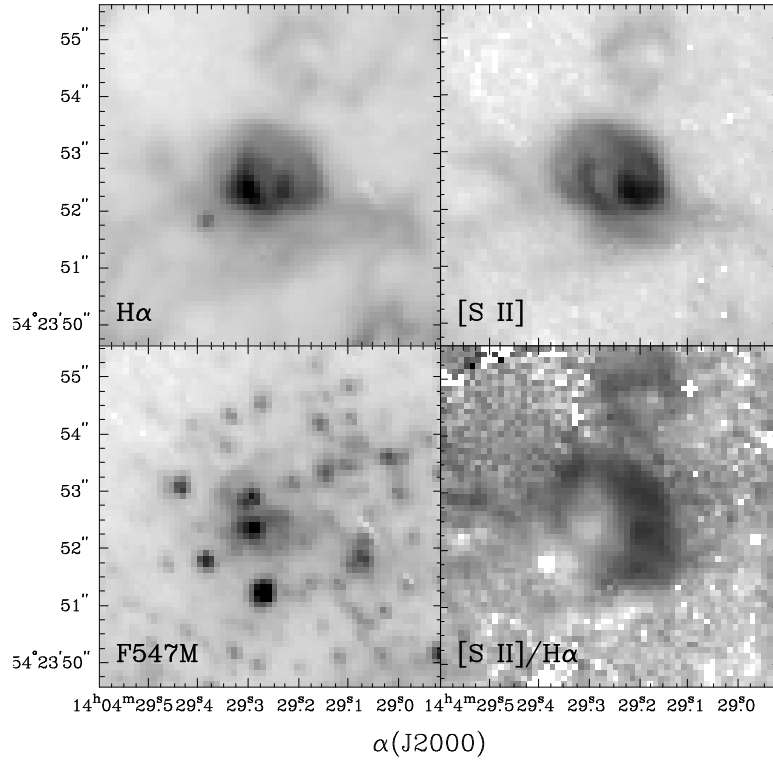


FIGURE 6. HST WFPC2 images of NGC 5471B in $H\alpha$ (F656N) and $[S II]$ (F673N) lines and a blue continuum (F547M) band. The lower right panel is the $[S II]/H\alpha$ ratio map. The $H\alpha$ image shows the ionized gas, $[S II]$ image the shocked gas, and the F547M image the stars. The brightest concentrations of stars are OB associations or clusters.

1999. These new spectra are deeper and have higher S/N than those presented by Chu & Kennicutt (1986). The new echelle data are analyzed similarly. As shown in Figure 7, the $H\alpha$ velocity profile can be fitted by two Gaussian components, with the broad component corresponding to SNR emission and the narrow component the background

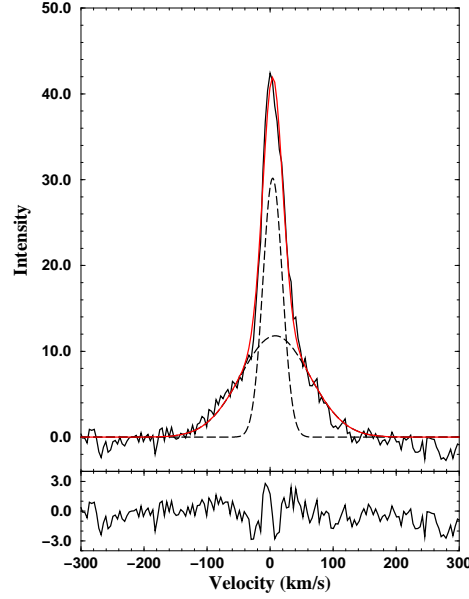


FIGURE 7. $H\alpha$ line profile of NGC 5471B. The profile is fitted by two Gaussian components. The dashed curves are the two components. The bottom panel plots the residuals.

HII region emission. The broad component contributes to $\sim 70\%$ of the total flux. Its FWHM is $135 \pm 5 \text{ km s}^{-1}$, but the faint wings extend over $\pm 210 \text{ km s}^{-1}$.

The $H\alpha$ luminosity of the SNR in NGC 5471B can be determined using the $H\alpha$ flux derived from the HST WFPC2 $H\alpha$ image, the broad/total flux ratio derived from the $H\alpha$ velocity profile, and the extinction derived spectroscopically by Kennicutt & Garnett (1996). The luminosity of the SNR so derived is $1.6 \times 10^{39} \text{ ergs s}^{-1}$. Assuming that the SNR shell has a shell thickness 1% of the shell radius, we derive a mass of $1.8 \times 10^4 M_{\odot}$. Adopting an expansion velocity of 210 km s^{-1} (one half of the full velocity extent), we derive a shell kinetic energy of $8.2 \times 10^{51} \text{ ergs}$. This kinetic energy is more than one order of magnitude higher than those seen in SNRs in the Magellanic Clouds (Williams et al. 1997, 1999). If the SNR in NGC 5471B is indeed a SNR caused by one single supernova explosion, the shell kinetic energy implies that the supernova explosion energy must be 3–30 times higher, depending on whether Sedov’s solution or Chevalier’s (1974) model is adopted. An explosion energy of $2 \times 10^{52} - 2 \times 10^{53} \text{ ergs}$ is 1–2 orders of magnitude higher than the canonical explosion energy of 10^{51} ergs (Jones et al. 1998).

A crucial question to ask is whether the energetic, expanding shell in NGC 5471B is indeed energized by a single supernova with an extraordinary explosion energy or a large number of stars over a long period of time. As the shell interior does not have a high concentration of stars and the [S II]-bright part of the shell is particularly devoid of stars, it is quite likely that the shell structure is a SNR, instead of a well-developed superbubble recently energized by an interior supernova. Further discussion is given in Section 8.

7. The Super-luminous SNR MF83 in M101

The super-luminous SNR MF83 was cataloged by Matonick & Fesen (1997). $H\alpha$ and V-band images of MF83 and surrounding regions have been obtained with the MDM 2.4m telescope by Eva Grebel, who has kindly made these images available to us. Figure 8 shows that MF83 is located between two spiral arms on the eastern part of M101. The

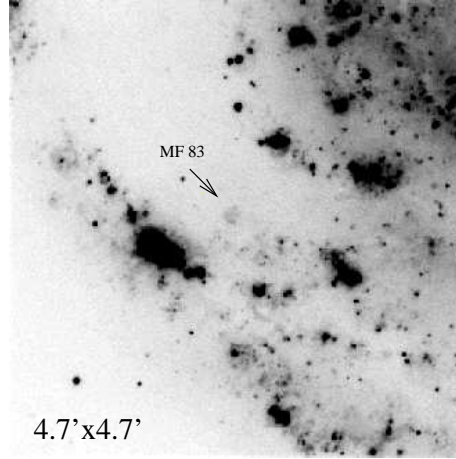


FIGURE 8. MDM 2.4m $H\alpha$ image of MF83 and the eastern portion of M101. (Photo credit: Eva Grebel)

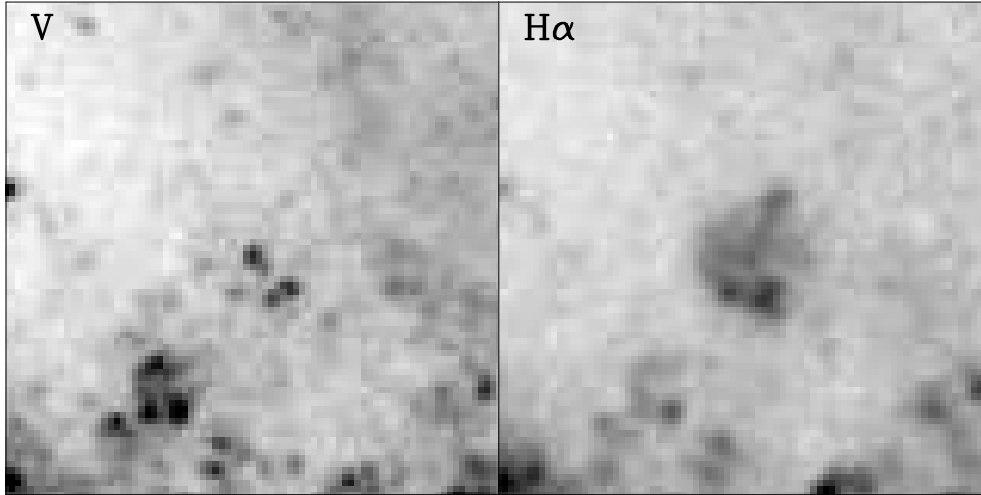


FIGURE 9. MDM 2.4m images of MF83 in the V-band and the $H\alpha$ line. The field of view is $45'' \times 45''$. (Photo credit: Eva Grebel)

$H\alpha$ image in Figure 9 shows that this remnant does not have a clear shell morphology. The bright spots on the south rim of the remnant corresponds to stars, which are better seen in the V-band image in Figure 9.

We have obtained high-dispersion echelle spectra of MF83 with the KPNO 4m telescope in 1999. The echelle observations detected MF83 in $H\alpha$, [N II], and [S II] lines. The $H\alpha$ line, having the highest S/N ratio, is displayed in Figure 10. The line image shows clearly an expanding shell structure, with the extreme velocities extending over $\sim 145 \text{ km s}^{-1}$. The integrated $H\alpha$ velocity profile of MF83, after subtracting the telluric OH line, can be fitted with a Gaussian component with a FWHM of $82 \pm 14 \text{ km s}^{-1}$ (see Figure 11). We adopt the full extent of the $H\alpha$ profile as twice the expansion velocity. The expansion velocity is thus $\sim 70 \text{ km s}^{-1}$.

We adopt the $H\alpha$ luminosity $1.7 \times 10^{38} \text{ ergs s}^{-1}$ from Matonick & Fesen (1997) and a diameter of 267 pc for MF83. Assuming a shell geometry with a shell thickness of 1%

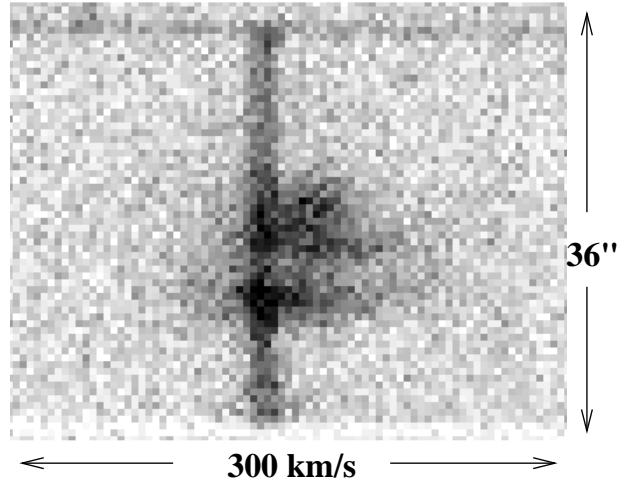


FIGURE 10. KPNO 4m echelle image of the H α line. The emission from MF83 shows a position-velocity ellipse indicating an expanding-shell structure. The narrow, constant component is a telluric OH line.

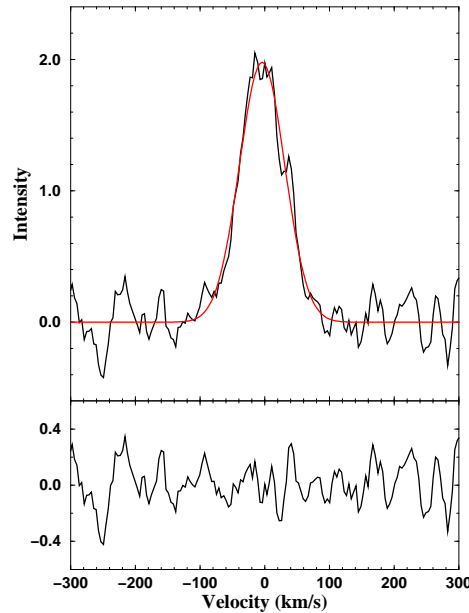


FIGURE 11. Integrated H α velocity profile of MF83. The superposed telluric OH line has been removed. The smooth curve is the Gaussian fit. The residuals are plotted in the bottom panel.

the shell radius, we derive a shell mass of $5.5 \times 10^4 M_{\odot}$ and a kinetic energy of 3×10^{51} ergs. If MF83 is formed by one single supernova explosion, the explosion energy would need to be 10^{52} – 10^{53} ergs. This is 1–2 orders of magnitude higher than the canonical explosion energy for a normal supernova.

Is MF83 formed by one single supernova? The answer is likely to be negative because (1) MF83 has a cluster at its center, (2) MF83's shell size is comparable to those of superbubbles around OB associations or clusters, and (3) MF83's shell expansion velocity is too low to produce X-ray emission. This will be discussed further in the next section.

Parameter	NGC 5471B	MF83	Units
Size	60	270	pc
V_{exp}	210	70	km s^{-1}
Mass	1.8×10^4	5.5×10^4	M_{\odot}
$L(\text{H}\alpha)$	1.6×10^{39}	1.7×10^{38}	ergs s^{-1}
$L(\text{X})$	1.7×10^{37}	1×10^{37}	ergs s^{-1}
Kinetic Energy	8×10^{51}	3×10^{51}	ergs
Explosion Energy	$2 \times 10^{52} - 2 \times 10^{53}$	$10^{52} - 10^{53}$	ergs
Radio spectrum	nonthermal	?	
X-ray spectrum	soft	?	
OB association	off-center	at center	
Powerful Explosion	very likely	less likely	

TABLE 3. Physical Properties of NGC 5471B and MF83

8. Are NGC 5471B and MF83 Remnants Related to GRBs?

It has been suggested that NGC 5471B and MF83 are hypernova remnants that require explosion energies comparable to the energies frequently associated with GRBs (Wang 1999). We have analyzed these two remnants using HST WFPC2 images, MDM 2.4m CCD images, and KPNO 4m echelle spectra. The results of our analysis are summarized in Table 3. While we find that the kinetic energies of these two remnants do require explosion energies of $10^{52} - 10^{53}$ ergs, we also find that they are in complex environments which make it difficult to assess whether they were formed by single supernova explosions.

NGC 5471B has nonthermal radio emission and soft X-ray emission that are characteristic of SNRs. It has an OB association/cluster at its rim, but its shell size is smaller than most known superbubbles. It is unlikely that the NGC 5471B shell is a superbubble produced by this off-center OB association/cluster. There is no obvious counter-evidence for the super-luminous SNR NGC 5471B to be produced by a single explosion. We consider that a single explosion is at least as likely as multiple explosions.

MF83, on the other hand, is not a known nonthermal radio source, and its ROSAT X-ray observations were too noisy to provide spectral information. It has an OB association/cluster at its center and its shell size is comparable to those commonly seen in superbubbles. MF83 was initially identified as a SNR based on its high [S II]/H α ratio, but many superbubbles are known to have high [S II]/H α ratios as well, e.g., N185 and N186E in the Large Magellanic Cloud (Lasker 1977). Its expansion velocity is on the high side of the known expansion velocities of superbubbles, but is similar to that of the aforementioned [S II]-bright superbubble N185 ($70 \pm 10 \text{ km s}^{-1}$, Rosado et al. 1982) and is too low to generate much X-ray emission. We therefore conclude that there is no compelling evidence for MF83 to be produced by one single powerful hypernova explosion.

Finally, are NGC 5471B and MF83 remnants of GRBs? The explosion energies we have derived have large uncertainties; however, the lower end of the energy range, a few times 10^{52} ergs, is compatible with some supernova energies determined recently by Branch (1999, this volume). We conclude that the association of these two super-luminous SNRs with GRBs is at best remote.

REFERENCES

- BLAIR, W. P. & FESEN, R. A. 1994 The Optical Counterpart to the Luminous X-ray Supernova Remnant in NGC 6946. *ApJ* **424**, L103–L106.
- BLAIR, W. P. & FESEN, R. A. 1998 New Constraints on the Age of the Ultraluminous Supernova Remnant in NGC 4449. *AAS* **193**, 74.04.
- BLAIR, W. P., FESEN, R. A., & SCHLEGEL, E. M. 1997 HST/WFPC2 Images of the Ultraluminous Supernova Remnant in NGC 6946. *AAS* **190**, 27.06.
- BLAIR, W. P., KIRSHNER, R. C., & WINKLER, P. F. 1983 The Extraordinary Extragalactic Supernova Remnant in NGC 4449. II. X-ray and Optical Investigations. *ApJ* **272**, 84–91.
- BLAIR, W. P. & LONG, K. S. 1997 Identification of Supernova Remnants in the Sculptor Group Galaxies NGC 300 and NGC 7793. *ApJS* **108**, 261–277.
- CHEVALIER, R. A. 1974 The Evolution of Supernova Remnants. I. Spherically Symmetric Models. *ApJ* **188**, 501–516.
- CHU, Y.-H. & KENNICUTT, R. C., JR. 1986 Kinematic Detection of Supernova Remnants in Giant HII Regions. *ApJ* **311**, 85–97.
- CHU, Y.-H. & KENNICUTT, R. C., JR. 1988 Echelle observations of Supernova Remnants in the Magellanic Clouds. *AJ* **95**, 1111–1121.
- D’ODORICO, S., DOPITA, M. A. & BENVENUTI, P. 1980 A Catalogue of Supernova Remnant Candidates in Nearby Galaxies. *A&AS* **40**, 67–80.
- DUNNE, B. C., GRUENDL, R. A., & CHU, Y.-H. 1999 What Produced the Ultraluminous Supernova Remnant in NGC 6946. *AAS* **194**, 85.05.
- GREEN, D. A. 1988 A Revised Reference Catalogue of Galactic Supernova Remnants. *Ap&SS* **148**, 3–74.
- JONES, T. W. ET AL. 1998 10^{51} Ergs: The Evolution of Shell Supernova Remnants. *PASP* **110**, 125–151.
- KENNICUTT, R. C., JR. & GARNETT, D. R. 1996 The Composition Gradient in M101 Revisited. I. HII Region Spectra and Excitation Properties. *ApJ* **456**, 504–518.
- KIRSHNER, R. C. & BLAIR, W. P. 1980 The Extraordinary Extragalactic Supernova Remnant in NGC 6946. *ApJ* **236**, 135–142.
- LASKER, B. M. 1977 Emission Nebulae with Strong [S II] in the Large Magellanic Cloud. *ApJ* **212**, 390–395.
- MATHEWSON, D. S., FORD, V. L., DOPITA, M. A., TUOHY, I. R., LONG, K. S., & HELFAND, D. J. 1983 Supernova Remnants in the Magellanic Clouds. *ApJS* **51**, 345–355.
- MATHEWSON, D. S., FORD, V. L., DOPITA, M. A., TUOHY, I. R., MILLS, B. Y., & TURTLE, A. J. 1984 Supernova Remnants in the Magellanic Clouds. *ApJS* **55**, 189–210.
- MATHEWSON, D. S., FORD, V. L., TUOHY, I. R., MILLS, B. Y., & TURTLE, A. J. 1985 Supernova Remnants in the Magellanic Clouds. III. *ApJS* **58**, 197–200.
- MATONICK, D. M. & FESEN, R. 1997 Optically Identified Supernova Remnants in the Nearby Spiral Galaxies: NGC 5204, NGC 5585, NGC 6946, M81, and M101. *ApJS* **112** 49–107.
- ROSADO, M., GEORGELIN, Y. M., GEORGELIN, Y. P., LAVAL, A., & MONNET, G. 1982 Kinematics of Ring-Shaped Nebulae in the LMC. II. The Radial Velocity Field of N185. *A&A* **115**, 61–64.
- SCHLEGEL, E. M. 1994 The Very Luminous Supernova Remnant in NGC 6946. *ApJ* **424**, L99–L102.
- SEAQUIST, E. R. & BIGNELL, R. C. 1978 Radio emission from a possible supernova remnant in the galaxy NGC 4449. *ApJ* **226**, L5–L6.
- SKILLMAN, E. D. 1985 Spatial Variation in the Physical Conditions in the Giant Extragalactic HII Region NGC 5471. *ApJ* **290**, 449–461.
- SMITH, R. C., ET AL. 1999 The UM/CTIO Magellanic Cloud Emission-line Survey. In *New Views of the Magellanic Clouds* (ed. Y.-H. Chu et al.). IAU Symposium No. 190, in press.
- VAN DYK, S. D., SRAMEK, R. A., WEILER, K. W., HYMAN, S. D., & VIRDEN, R. E. 1994 The Radio Counterpart to the Luminous X-ray Supernova Remnant in NGC 6946. *ApJ* **425**,

L77–L79.

WANG, Q. D. 1999 Detection of X-Ray-emitting Hypernova Remnants in M101. *ApJ* **517** L27–L30.

WILLIAMS, R. M. & CHU, Y.-H. 1995 X-ray Emission from Giant HII Regions in M101. *ApJ* **439**, 132–144.

WILLIAMS, R. M., CHU, Y.-H., DICKEL, J. R., BEYER, R., PETRE, R., SMITH, R. C., & MILNE, D. K. 1997 Supernova Remnants in the Magellanic Clouds. I. The Colliding Remnants DEM L316 *ApJ* **480**, 618–632.

WILLIAMS, R. M., CHU, Y.-H., DICKEL, J. R., SMITH, R. C., MILNE, D. K., & WINKLER, P. F. 1999 Supernova Remnants in the Magellanic Clouds. II. Supernova Remnant Breakouts from N11L and N86. *ApJ* **514**, 798–817.